Characterizing cerebral hemodynamics across the adult lifespan with arterial spin labeling MRI data from the Human Connectome Project-Aging

Meher R. Juttukonda[a,b,*], **Binyin Li**[a,c], **Randa Almaktoum**[a], **Kimberly A. Stephens**[a], **Kathryn M. Yochim**[a], **Essa Yacoub**[g], **Randy L. Buckner**[a,d,e], **David H. Salat**[a,b,f]

[a]Athinoula A. Martinos Center for Biomedical Imaging, Department of Radiology, Massachusetts General Hospital, 149 Thirteenth Street, Suite, 2301, Charlestown 02129, MA, United States

[b]Department of Radiology, Harvard Medical School, Boston, MA, United States

[c]Department of Neurology, Ruijin Hospital & Shanghai Jiao Tong University School of Medicine, Shanghai, China

[d]Department of Psychology, Harvard University, Cambridge, MA, United States

[e]Department of Neuroscience, Harvard University, Cambridge, MA, United States

[f]Neuroimaging Research for Veterans Center, VA Boston Healthcare System, Boston, MA, United States

[g]Center for Magnetic Resonance Research, Department of Radiology, University of Minnessota, Minneapolis, MN, United States

Abstract

Arterial spin labeling (ASL) magnetic resonance imaging (MRI) has become a popular approach for studying cerebral hemodynamics in a range of disorders and has recently been included as part of the Human Connectome Project-Aging (HCP-A). Due to the high spatial resolution and multiple post-labeling delays, ASL data from HCP-A holds promise for localization of hemodynamic signals not only in gray matter but also in white matter. However, gleaning information about white matter hemodynamics with ASL is challenging due in part to longer blood arrival times in white matter compared to gray matter. In this work, we present an analytical

*Corresponding author at: Athinoula A. Martinos Center for Biomedical Imaging, Massachusetts General Hospital, 149 Thirteenth Street, Suite 2301, Charlestown 02129, MA, Phone: 617-724-0844. mjuttukonda@mgh.harvard.edu (M.R. Juttukonda).

approach for deriving measures of cerebral blood flow (CBF) and arterial transit times (ATT) from the ASL data from HCP-A and report on gray and white matter hemodynamics in a large cohort (n = 234) of typically aging adults (age 36–90 years). Pseudo-continuous ASL data were acquired with labeling duration = 1500 ms and five post-labeling delays = 200 ms, 700 ms, 1200, 1700 ms, and 2200 ms. ATT values were first calculated on a voxel-wise basis through normalized cross-correlation analysis of the acquired signal time course in that voxel and an expected time course based on an acquisition-specific Bloch simulation. CBF values were calculated using a two-compartment model and with age-appropriate blood water longitudinal relaxation times. Using this approach, we found that white matter CBF reduces ($\rho = 0.39$) and white matter ATT elongates ($\rho = 0.42$) with increasing age ($p < 0.001$). In addition, CBF is lower and ATTs are longer in white matter compared to gray matter across the adult lifespan (Wilcoxon signed-rank tests; $p < 0.001$). We also found sex differences with females exhibiting shorter white matter ATTs than males, independently of age (Wilcoxon rank-sum test; $p < 0.001$). Finally, we have shown that CBF and ATT values are spatially heterogeneous, with significant differences in cortical versus subcortical gray matter and juxtacortical versus periventricular white matter. These results serve as a characterization of normative physiology across the human lifespan against which hemodynamic impairment due to cerebrovascular or neurodegenerative diseases could be compared in future studies.

1. Introduction

Arterial spin labeling (ASL) magnetic resonance imaging (MRI) is a noninvasive technique for measuring tissue-level hemodynamics (Williams et al., 1992). For neurological applications, the magnetization of arterial blood water in the neck is inverted with either a single adiabatic radiofrequency pulse (Wong et al., 1997) (pulsed ASL) or with a long train of short, Hanning-windowed block pulses (Dai et al., 2008) (pseudo-continuous ASL; pCASL). Images of the brain containing this magnetic label ('label' state) are then acquired following a delay that allows the labeled blood to reach and perfuse brain tissue (i.e., post-labeling delay; PLD). The difference between these 'label' images and images acquired without radiofrequency inversion ('control' state) is proportional to cerebral blood flow (CBF), and this difference signal is used to extract CBF.

Due to its quantitative and noninvasive nature, ASL has become a popular approach for studying cerebral hemodynamics in health and also in a range of cerebrovascular (Donahue et al., 2017; Wang et al., 2020; Bastos-Leite et al., 2008; van Dalen et al., 2016; Bahrani et al., 2017), neurodegenerative (Thomas et al., 2019; Dolui et al., 2020), and psychiatric disorders (Cooper et al., 2019). This rise in popularity over the past decade led to the release of a consensus statement from the Perfusion Study Group of the International Society on Magnetic Resonance in Medicine, which provided guidelines for acquisition and processing of ASL data for clinical use (Alsop et al., 2015). Due to the limitations associated with more advanced approaches at the time, these guidelines were initially focused on ASL data acquired with a single PLD. However, ASL images can now be reasonably acquired with multiple PLDs, allowing for simultaneous measurement of both CBF and arterial transit time (ATT), which represents the time it takes for labeled blood to reach brain tissue. While much effort has been focused on understanding CBF, ATT also provides interesting physiological

information (Mutsaerts et al., 2017). Delays in ATT are characteristic of steno-occlusive cerebrovascular diseases (Hendrikse et al., 2004) and may also affect CBF computation if not measured and accounted for (Hirschler et al., 2018). Additionally, ATTs are thought to increase with age (Liu et al., 2012) and may be adversely affected by aging-related disorders, including dementia (Mak et al., 2012). Thus, multi-delay ASL protocols that can provide robust measures of both CBF and ATT, allowing for optimization of regional CBF modeling based on ATT, are of broad interest.

Multi-PLD schemes were initially limited by increased acquisition times, but recent advances have allowed for multiple PLDs to be acquired efficiently and quickly, including with the use of simultaneous multi-slice (SMS) imaging (Eichner et al., 2014). Multi-PLD ASL protocols incorporating these advances have been included as part of the imaging protocol in the Human Connectome Project-Aging (HCP-A) (Harms et al., 2018) to understand age-related changes in gray matter hemodynamic function. In addition, ASL data from HCP-A may also hold promise for localization of hemodynamic signals in white matter, as the high spatial resolution utilized allows for reduced partial volume effects and better isolation of these tissues. As the critical role of white matter in maintaining proficient cognitive and behavioral function is being increasingly recognized (Filley and Fields, 2016), the ability to measure microvascular properties in white matter may be significant for understanding the link between vascular and cognitive function. However, gleaning information about white matter hemodynamic function with ASL has been challenging due to the lower vascular density and longer ATTs in white matter compared to gray matter. Thus, an approach to quantification that can quantify physiology in the presence of such longer transit times is necessary.

In this work, we first present an approach for computing ATT in brain regions from which these parameters can be feasibly measured based on temporal signal properties in the multi-PLD HCP-A data. We then apply this approach to report cross-sectional findings of age and sex effects on gray and white matter ATT and CBF, as well as potential impacts of spatial location on these hemodynamic properties.

2. Materials and methods

2.1. Study participants

Adult participants ($n = 234$; 55.6% female) who exhibited typical health for their age without stroke, clinical dementia, or other identified causes of cognitive decline were enrolled through the Brain Aging and Dementia Laboratory at Massachusetts General Hospital (MGH) as part of HCP-A (Harms et al., 2018; Bookheimer et al., 2019; Somerville et al., 2018). All participants provided informed, written consent for this Institutional Review Board-approved cross-sectional study. After consent was provided, the Montreal Cognitive Assessment was administered, and participants meeting the determined threshold for their age were deemed eligible for the study. Data from participants older than 90 years of age were excluded from this report due to privacy concerns. No participants were excluded based on medication use, but self-reported prescription or over-the-counter medication use was recorded at the time of the study visit. More details regarding these cognitive assessments as well as additional inclusion and exclusion criteria for HCP-A have

been described previously (Bookheimer et al., 2019). Demographic variables, including age, sex, race, and ethnicity are summarized in Table 1. In addition, the medication use, including anti-hypertensive medications that could affect hemodynamics, is also documented in Table 1.

2.2. Data acquisition

MR images were acquired with a 3.0 Tesla Prisma scanner (Siemens; Erlangen, Germany) using a 32-channel head coil. T_1-weighted imaging was performed using multi-echo MPRAGE and with the following parameters: TR = 2500 ms; TI = 1000 ms; TE = 1.8/3.6/5.4/7.2 ms; spatial resolution = $0.8 \times 0.8 \times 0.8$ mm^3; number of echoes = 4. pCASL data were acquired without background suppression as previously described (Li et al., 2018) with labeling duration (τ) = 1500 ms and five post-labeling delays (PLD) = 200 ms (control/label pairs = 6), 700 ms (pairs = 6), 1200 ms (pairs = 6), 1700 ms (pairs = 10), and 2200 ms (pairs = 15). Signal readout was performed using multi-band 2D gradient echo echo-planar imaging (EPI) with the following parameters: TR = 3580 ms; TE = 19 ms; partial Fourier = 6/8; SMS acceleration factor = 6; total slices = 60; spatial resolution = $2.5 \times 2.5 \times 2.5$ mm^3; total acquisition time = 5.5 min. Two equilibrium magnetization (M_0) images were acquired at the end of the scan. A pair of spin echo EPI scans with opposite phase encoding directions were also acquired for use in the correction of field inhomogeneity-related distortions: TR = 8000; TE = 40 ms; spatial resolution = $2.5 \times 2.5 \times 2.5$ mm^3.

2.3. Physiological image pre-processing

ASL data were corrected for susceptibility distortions using the spin echo EPI data and with 'TopUp' (Andersson et al., 2003) (FSL (Smith et al., 2004); FMRIB; Oxford, United Kingdom). Signal loss that occurred due to spin history effects from the multi-band readout was addressed by interpolating the last slice of each band using the slices positioned immediately on either side (see "Discussion"). Motion correction was performed using in-house routines. Control and label ASL data were pair-wise subtracted, averaged for each PLD, and normalized to the second M_0 image.

2.4. Structural image processing

T_1-weighted anatomical images were automatically processed to reconstruct cortical surfaces and to segment region of interest (ROI) volumes using the FreeSurfer recon-all procedure (http://surfer.nmr.mgh.harvard.edu/) (Dale et al., 1999; Fischl et al., 1999). Control ASL images were registered to T_1-weighted image space using a boundary-based registration algorithm (Greve and Fischl, 2009), and the inverse transform was used to transform gray and white matter masks into ASL space. White matter signal abnormalities, potentially indicative of white matter lesions, were segmented separately and were not included in the white matter mask.

2.5. Arterial transit time

ATT values were calculated on a voxel-wise basis through a two-stage normalized cross-correlation approach. First, the measured signal time course in a voxel (i.e., acquired) was cross-correlated with a time course obtained via simulation of the flow-modified Bloch

equation as described previously (Juttukonda et al., 2017) with ATT = 1.2 s and down-sampled to match the temporal resolution of the acquired ASL data (Fig. 1 A). Cross-correlation analysis was performed using the 'xcorr' function (with the 'coeff' normalization option) in MATLAB (The Mathworks; Natick, MA, USA) between the simulated and acquired signal time courses at 11 shift indices ranging between − 5 to + 5 (Fig. 1 B). The maximum correlation between the acquired and simulated time courses and the corresponding time shift were recorded for each intracranial imaging voxel (Fig. 1 C). Next, ATT values were assigned based on a second cross-correlation analysis, where the measured time course in a voxel was cross-correlated with simulated time courses generated with a temporal resolution = 0.1 s for ATTs between 0.2 s and 3.2 s. The simulated curve that produced the maximum correlation within the bounds defined for each shift index was used to determine the ATT in each voxel (Section 3.1). Results validating this approach are presented as Supplementary Material.

2.6. Cerebral blood flow

CBF values were calculated using a previously described two-compartment model (Fan et al., 2017) (Eq. (1)) at each PLD, i:

$$CBF_i = \frac{6000 \cdot \lambda \cdot \Delta M_i \cdot \exp\left(\frac{\delta}{T_{1,a}}\right)}{2 \cdot \alpha \cdot M_0 \cdot T_{1,a} \cdot \left[\exp\left(-\frac{\max(PLD_i - \delta, 0)}{T_{1,t}}\right) - \exp\left(-\frac{\max(\tau + PLD_i - \delta, 0)}{T_{1,t}}\right)\right]},$$

where $\lambda = 0.9$ g/ml is the blood-brain partition coefficient, M_i is the ASL difference signal in each voxel, $\alpha = 0.85$ is the labeling efficiency, M_0 is the equilibrium magnetization in each voxel, $T_{1,a}$ is the longitudinal relaxation of arterial blood, $T_{1,t} = 1.2$ s is the longitudinal relaxation time of tissue, PLD_i is the post-labeling delay (after slice timing correction), $\tau = 1.5$ s is the labeling duration, and δ is the ATT in each voxel. $T_{1,a}$ was calculated on an individual basis using a previously characterized relationship (Lu et al., 2004) (Eq. (2)):

$$T_{1,a} = \frac{1}{0.52 \cdot Hct + 0.38},$$

where Hct is the hematocrit. For each participant, a hematocrit value appropriate for age and sex (Mahlknecht and Kaiser, 2010) was used, as these values were not available as part of the HCP-A study. A final CBF map was derived for each participant in a voxel-wise manner as the average of the CBF values at each PLD_i where $PLD_i + \tau >$ ATT, ensuring that CBF estimates are calculated using as much information from the multi-PLD scans as appropriate (Dai et al., 2017).

2.7. Analysis of hemodynamic physiology

To understand relationships between age, sex and tissue-level hemodynamics, mean CBF and ATT were computed in gray matter and white matter for each participant using tissue masks derived based on structural images processed with FreeSurfer (Dale et al., 1999). First, the association between these values and age was assessed in all participants. Next, participants were divided into quartiles by age, and CBF and ATT were compared between

gray and white matter separately for each age group. Third, participants were stratified by sex, and CBF and ATT values were compared between males and females for gray and white matter separately. Lastly, a multivariate regression was performed for each hemodynamic variable to assess the effects of age and sex, as well as the interaction between the two.

To examine potential spatial variations, mean CBF and ATT were also calculated inside of gray and white matter subtypes. Gray matter was subdivided into cortical and subcortical subregions, and white matter was subdivided into juxtacortical and periventricular volumes, again using FreeSurfer-based segmentations. The subcortical gray matter segmentation was composed of the following structures: thalamus, caudate, putamen, pallidum, hippocampus, and amygdala. To reduce partial volume-related contamination, the white matter mask and subcortical gray matter masks were eroded using a disk-shaped element with a radius of 5 mm.

Finally, to understand how gray and white matter hemodynamic physiology may be coupled and how such coupling may be associated with age, we compared CBF and ATT in white versus gray matter separately for each quartile of age.

2.8. Statistical considerations

Continuous variables are described using the median and interquartile range (IQR). Categorial variables are presented as percentages and compared using the Chi-squared test of proportions. Comparisons of medians between two continuous variables were performed using the Wilcoxon rank-sum test (for unpaired comparisons) or using the Wilcoxon signed-rank test (for paired comparisons). Comparisons of continuous variables across more than two categorical variables were performed using the Jonckheere-Terpstra trend test. Associations between continuous variables were assessed using Spearman's rank correlation analysis. All statistical tests were performed at a 0.05 level of significance.

3. Results

Data from 234 participants in the local MGH HCP-A cohort (median age = 61 years; 55% female) were analyzed for this study. The quartiles of age were divided as follows: Q1 = 36–49 years; Q2 = 49–61 years; Q3 = 61–77 years; Q4 = 77–90 years.

3.1. Computation of ATT and CBF

Initial cross-correlation analysis showed that 10 shift indices produced non-zero maximum correlations with the simulation, and shift indices ranging from − 4 to + 2 exhibited the expected kinetic curve shapes (Fig. 2 A). The range of ATTs searched in the second stage was determined based on these shift indices. For voxels with shift = 0, the searched range was between 0.9 s and 1.5 s. For voxels with positive shift indices (i.e., shift=+1 and shift= +2), the range of ATTs searched was between 0.2 s and 1.2 s. For voxels with negative time shifts (i.e., shift = − 1 to − 4), the range of ATTs searched was between 1.2 s and 3.2 s. Meanwhile, shifts ranging from + 3 to + 5 theoretically corresponded to negative ATTs, which are physiologically unmeaningful (Fig. 2 B). In addition, voxels corresponding to these indices were typically present in regions where no ASL signal is expected (i.e., CSF) or regions where ATTs are typically very delayed (i.e., deep white matter). Therefore, voxels

with these shift indices (+ 3 to + 5) were empirically assigned ATT = 3.3 s. Finally, shift index = − 5 was not assigned to any voxels as there was no overlap between the theoretical model and acquired data at this shift. This resulted in voxel-wise ATT maps with a temporal resolution of 0.1 s, which were then used to compute CBF using a two-compartment model (Section 2.6).

3.2. Hemodynamic physiology and age

CBF was inversely associated with age, and older age correlated with lower CBF in both gray ($p < 0.001$) and white ($p < 0.001$) matter, but this relationship was stronger in gray (Spearman's $\rho = − 0.49$) versus white (Spearman's $\rho = − 0.39$) matter. CBF in gray matter was higher than CBF in white matter in participants across all four quartiles of age. For Q1, gray matter CBF was 60.2 [51.8, 67.5] ml/100 g/min, while white matter CBF was 21.7 [19.7, 23.5] ml/100 g/min ($p < 0.001$). For Q2, gray matter CBF was 58.7 [52.2, 64.4] ml/100 g/min, and white matter CBF was 22.8 [20.6, 24.5] ml/100 g/min ($p < 0.001$). For Q3, gray matter CBF was 51.0 [45.9, 56.8] ml/100 g/min, and white matter CBF was 20.7 [18.5, 23.4] ml/100 g/min ($p < 0.001$). For Q4, gray matter CBF was 43.8 [38.2, 53.6] ml/100 g/min, while white matter CBF was 18.2 [16.0, 19.9] ml/100 g/min ($p < 0.001$). CBF results are graphically illustrated in Fig. 3.

ATT was directly associated with age, and older age correlated with longer ATT in both gray ($\rho = 0.56$; $p < 0.001$) and white ($\rho = 0.42$; $p < 0.001$) matter. ATT was longer in white matter than in gray matter across all four quartiles of age. For Q1, gray matter ATT was 1.28 s [1.09 s, 1.44 s], while white matter ATT was 1.69 s [1.58 s, 1.83 s] ($p < 0.001$). For Q2, gray matter ATT was 1.33 s [1.22 s, 1.52 s], and white matter ATT was 1.75 s [1.64 s, 1.85 s] ($p < 0.001$). For Q3, gray matter ATT was 1.55 s [1.37 s, 1.68 s], and white matter ATT was 1.86 s [1.74 s, 1.94 s] ml/100 g/min ($p < 0.001$). For Q4, gray matter ATT was 1.63 s [1.48 s, 1.77 s], while white matter ATT was 1.87 s [1.80 s, 1.97 s] ($p < 0.001$). Group-level ATT results are illustrated in Fig. 4.

The ratio of gray-to-white matter CBF decreases with age ($p < 0.001$), with the youngest subjects exhibiting the highest ratio (Q1; ratio = 2.85) and the oldest subjects exhibiting the lowest ratio (Q4; ratio = 2.44) (Fig. 5 A). The ratio of gray-to-white matter ATT increases with age ($p < 0.001$), with the youngest subjects exhibiting the lowest ratio (Q1; ratio = 0.75) and the oldest subjects exhibiting the lowest ratio (Q4; ratio = 0.87) (Fig. 5 B).

3.2. Sex differences in CBF and ATT

There was no significant difference in age between male (age = 62 [50, 78] years) and female (age = 58 [47, 77]) participants in this study ($p = 0.33$). Gray matter CBF was significantly higher in females (CBF = 57.8 [50.4, 64.3] ml/100 g/min) than in males (CBF = 50.2 [42.3, 57.5] ml/100 g/min; $p < 0.001$). White matter CBF was also significantly higher in females (CBF = 21.2 [19.4, 24.2] ml/100 g/min) than in males (CBF = 20.1 [17.9, 22.4] ml/100 g/min; $p = 0.01$) (Fig. 6 A). Gray matter ATT was significantly higher in males (ATT = 1.59 s [1.40 s, 1.69 s]) than in females (ATT = 1.35 s [1.18 s, 1.54 s] ml/100 g/min; $p < 0.001$). Similarly, white matter ATT was significantly higher in males (ATT = 1.85 s [1.77 s, 1.97 s]) than in females (ATT = 1.74 s [1.60 s, 1.88 s] ml/100 g/min; $p < 0.001$)

(Fig. 6 A). Multivariate regression analysis confirmed these univariate analyses, showing that, independently of age, males had a lower gray matter CBF (estimate = − 13.9; $p = 0.01$), longer gray matter ATT (estimate = 0.35; $p < 0.001$), and longer white matter ATT (estimate = 0.27; $p < 0.001$). Unlike in the univariate analysis, males and females did not differ in white matter CBF (estimate = − 2.81; $p = 0.21$). Finally, there was a significant interaction between age and sex in white matter ATT, with females exhibiting a faster increase with age (estimate = 2.59×10^{-3}; $p = 0.02$) (Fig. 6 B).

3.3. Differences across tissue subtypes

Subregions within gray and white matter exhibited differences in CBF and ATT (Fig. 7). Cortical gray matter exhibited a higher CBF (CBF = 53.8 [46.3, 62.1] ml/100 g/min) compared to subcortical gray matter (CBF = 48.7 [42.8, 55.3] ml/100 g/min; $p < 0.001$). In addition, cortical gray matter exhibited longer ATTs (ATT = 1.46 s [1.26 s, 1.64 s]) compared to subcortical gray matter (ATT = 1.32 s [1.12 s, 1.50 s]; $p < 0.001$). Juxtacortical white matter (CBF = 21.4 [19.0, 24.1] ml/100 g/min) exhibited a higher CBF compared to periventricular white matter (CBF = 19.3 [17.1, 22.1] ml/100 g/min; $p < 0.001$). Meanwhile, periventricular white matter (ATT = 1.83 s [1.71 s, 1.95 s]) exhibited longer ATTs compared to juxtacortical white matter (ATT = 1.80 s [1.65 s, 1.90 s]; $p = 0.006$).

Representative examples showing that group-level differences in CBF and ATT across different age groups can also be visualized at the individual level are shown in Fig. 8.

4. Discussion

In this study, we present an approach for deriving measures of CBF and ATT across the lifespan with multi-PLD ASL MRI data acquired in the Human Connectome Aging Project. We used normalized cross-correlation analysis with simulations based on acquisition parameters to extract ATT. Next, we used these ATT values along with a two-compartment model to compute CBF at each PLD and combined these CBF values at PLD times longer than ATT. Using this approach, we have presented findings regarding normative cerebral hemodynamics and their association with age, sex, and tissue anatomy in a large ($n = 234$) cohort of adults (36–90 years). Our main findings were that CBF reduces and ATT elongates with increasing age in both gray and white matter. We also found that CBF is lower and ATT is longer in white matter when compared with gray matter across the lifespan. Finally, we demonstrated sex differences in white matter hemodynamic function as well as spatial heterogeneity in hemodynamics associated with sub-classes of gray and white matter. These results serve as a characterization of normative physiology against which hemodynamic impairment due to cerebrovascular or neurodegenerative diseases could be compared.

ASL MRI data acquired with multiple PLDs can be used to measure ATT in addition to CBF. To reliably extract ATT from kinetic model fitting of the multi-PLD data, sampling along both the ascending and descending portions of the kinetic curve is necessary. As ATT values in gray matter may be as low as 1.0 to 1.2 s, shorter pCASL labeling durations than recommended may be required to sensitize the signal to the ascending portion of the curve. However, lower labeling durations typically result in lower SNR, and potentially mitigate the SNR advantage of pCASL over other techniques, and so labeling durations of 1.5–1.8 s have

been recommended for use with pCASL sequences (Alsop et al., 2015). An alternate approach is to use a weighted-delay technique that utilizes an empirical relationship between ATT and PLD-weighted ASL difference signal (Dai et al., 2017). However, this approach may be affected by the range of PLD times acquired, and regions with particularly long ATT (longer than can be captured with the range of PLDs used) could be underestimated. The proposed approach overcomes these hurdles by allowing for measurement of ATT in regions where the ATT may be too long to measure with conventional approaches and in regions where sampling of the ascending portion of the kinetic curve may not be possible due to a long labeling duration. Overall, the mean gray matter (CBF = 54.4 ml/100 g/min) and white matter (CBF = 21.2 ml/100 g/min) CBF values across all participants (mean age = 62 years) with our approach align well with previously reported values measured with positron emission tomography in a similar age range (Buijs et al., 1998). Using this approach, we investigated relationships between global gray matter and white matter hemodynamics and demographic variables, including age and sex, and also how these relationships may differ in subregions of these tissues. Prior studies have investigated age effects on and sex differences in hemodynamic function (predominantly CBF) in the human brain (most commonly in gray matter). Here, we discuss the findings of our current study in the context of prior studies utilizing ASL-MRI and also emphasize findings regarding ATT and white matter that are potentially more novel.

First, we found that global gray matter CBF is inversely associated with age in a large cohort (n = 234) of adult participants spanning six decades (36–90 years old). Decreasing gray matter CBF with increasing age has been frequently reported with ASL (Mutsaerts et al., 2017; Liu et al., 2012; Asllani et al., 2009; Ambarki et al., 2015; Wagner et al., 2012; Taneja et al., 2020; De Vis et al., 2018; Zhang et al., 2017), and our gray matter CBF values (overall mean = 54.4 ml/100 g/min) and observed rate of decline (0.47% per year) are in good agreement with prior reports in middle-aged to older adults (Parkes et al., 2004; Biagi et al., 2007). While gray matter CBF changes in aging have been extensively studied, fewer studies using ASL-MRI have reported on changes in white matter CBF with aging (Parkes et al., 2004; Biagi et al., 2007), potentially due to the difficulties in measuring white matter perfusion with ASL. Here, we used an ASL processing approach specifically designed to enable quantification of signal from white matter. With this approach, we have shown that white matter CBF (overall mean = 21.2 ml/100 g/min) also significantly decreases with increasing age, but at a slower rate (0.34% per year) than in gray matter. This could indicate that age-effects on white matter CBF may be more difficult to detect than effects on gray matter CBF or that white matter microvasculature may potentially be more resilient to age effects (Thomas et al., 2014). In addition, we found that gray matter CBF was consistently higher than white matter CBF at all quartiles of age, but with decreases in the gray-to-white-matter ATT ratio with increasing age. However, decreases in CBF may not be uniform across the lifespan, and CBF has been shown to plateau in middle age after a sharp decline in the second decade of life (Biagi et al., 2007). Our results (Fig. 4 E, F) show a similar relationship with gray matter CBF being relatively stable and white matter CBF increasing until ~60 years of age, followed by declining CBF in older age.

Second, we found that global gray matter ATTs are directly associated with increasing age, a finding that is also in good agreement with previous studies using multi-delay ASL

(Mutsaerts et al., 2017; Liu et al., 2012; Dai et al., 2017; Campbell and Beaulieu, 2006). Importantly, we have provided novel evidence that elevations in white matter ATT are also significantly associated with increasing age. In addition, we found that white matter ATT was consistently higher than gray matter ATT at all quartiles of age, but with the magnitude of these differences reducing with increasing age. While the relationship between CBF and age may depend on decade of life, ATT increases appear to occur continuously throughout the lifespan. These findings may be relevant for identifying potential macrovascular mechanisms (slower blood velocity, increased vessel tortuosity, etc.) that contribute to increased risk for hemodynamic compromise in older adults and also for guiding the choice of PLD in single-delay ASL experiments in older populations and in studies targeting white matter.

Third, we observed differences in both gray and white matter in male and female participant groups. Gray matter CBF was higher in females compared with males, and gray matter ATT was longer in males compared to females. In white matter, ATT was longer in males compared to females, but there was no significant difference in CBF after accounting for age. The findings regarding CBF are in good agreement with what has been reported previously (Parkes et al., 2004; Smith et al., 2019; Liu et al., 2016), while the ATT findings provide more novel information. Shorter ATTs have previously been associated with elevated cervical arterial velocity in anemic adults (Juttukonda et al., 2017), which in turn is related to hematocrit. There are known sex differences in hematocrit (Devine, 1967), and thus, it is reasonable that arterial velocities may be higher in women, especially at younger ages where hematocrit differences are more pronounced, resulting in shorter ATTs in women than in men. These univariate analyses were also confirmed with a multivariate regression, which showed that both age and sex are independently associated with gray matter CBF, gray matter ATT, and white matter ATT, while only age is independently associated with white matter CBF. Importantly, these hemodynamic differences were observed even after correcting for potential hematocrit differences between the groups in the CBF quantification, which, if left uncorrected, may produce an artifactually-high CBF in women.

Fourth, changes in hemodynamic properties with age may be region-dependent, and both increases and decreases in relative CBF with age have been reported in various gray matter subregions (Zhang et al., 2018; Lee et al., 2009; Preibisch et al., 2011), indicating the importance of examining these parameters on a regional basis. When comparing subtypes of gray matter and white matter, we found a significant difference between cortical gray matter and subcortical gray matter, which is in good agreement with previous findings (Pavilla et al., 2016). We also observed a small but significant difference between CBF in juxtacortical white matter and periventricular white matter. Lower baseline perfusion in periventricular white matter could explain why this region is particularly vulnerable to white matter damage of presumed ischemic origin (De Reuck, 1971). When comparing subtypes of gray and white matter, we found that ATT in cortical gray matter was longer than in subcortical gray matter. In addition, ATT in periventricular white matter was significantly longer than in juxtacortical white matter. These findings are in agreement with a previous study which found that ATT in the basal ganglia is shorter than in cortical gray matter regions (Dai et al., 2017) and could be explained by known differences regarding the vascular supply between cortical and subcortical structures. Subcortical regions are supplied by perforating branches

of the middle cerebral and internal carotid arteries, including the anterior choroidal artery (Herman et al., 1966) and the lenticulostriate arteries (Herman et al., 1966), which branch off prior to the large arteries reaching cortical regions.

This study should be considered in the context of the following limitations. The multi-PLD ASL sequence in the HCP-A protocol incorporated state-of-the-art developments in acquisition techniques, including simultaneous multi-slice imaging. However, the use of SMS may result in signal voids at the edges of each imaging band due to spin history effects when the number of slices per band is even (Setsompop et al., 2012). These effects are exacerbated by the subtraction procedure in ASL and require a correction in post-processing. In this study, we addressed this by removing the affected slices and interpolating them using the slices immediately superior and inferior to the affected slice. While this may have adverse effects on the accuracy of the hemodynamic maps in these slices, they compose < 10% of the brain volume and are not expected to have a major impact on global measures. However, further work is necessary to understand how to best account for these effects. The study also exhibits the following strengths. First, the results of the study are reported from a sample size of 234 adults with a wide age range (36–90 years) represented. This allowed for the study of age effects on hemodynamic parameters in a large sample but also for the subdivision of the sample to compare gray and white matter physiology in different age groups. Second, the ASL sequence produced high-resolution images using a multi-band, multi-delay approach that were acquired in a clinically feasible acquisition time. The voxel size acquired with this sequence (2.5 mm isotropic) approaches the average thickness of the cerebral cortex (Fischl and Dale, 2000) and reduces the likelihood of partial volume contamination on measured tissue parameters.

In conclusion, we present a processing approach for deriving measures of ATT and CBF from multi-PLD ASL data acquired as part of HCP-A. Using this approach, we have demonstrated that CBF decreases and ATT elongates with age in white matter as well as in gray matter. Future work involves studying these measures as a function of imaging markers of vascular impairment, including white matter lesions.

Supplementary Material

Refer to Web version on PubMed Central for supplementary material.

Acknowledgments

References

Williams DS, Detre JA, Leigh JS, Koretsky AP, 1992. Magnetic resonance imaging of perfusion using spin inversion of arterial water. Proc. Natl. Acad. Sci. U. S. A 89, 212–216. [PubMed: 1729691]

Wong EC, Buxton RB, Frank LR, 1997. Implementation of quantitative perfusion imaging techniques for functional brain mapping using pulsed arterial spin labeling. NMR Biomed. 10, 237–249. [PubMed: 9430354]

Dai W, Garcia D, de Bazelaire C, Alsop DC, 2008. Continuous flow-driven inversion for arterial spin labeling using pulsed radio frequency and gradient fields. Magn. Reson. Med 60, 1488–1497. [PubMed: 19025913]

Donahue MJ, Juttukonda MR, Watchmaker JM, 2017. Noise concerns and post-processing procedures in cerebral blood flow (CBF) and cerebral blood volume (CBV) functional magnetic resonance imaging. Neuroimage 154, 43–58. [PubMed: 27622397]

Wang K, Shou Q, Ma SJ, Liebeskind D, Qiao XJ, Saver J, et al., 2020. Deep learning detection of penumbral tissue on arterial spin labeling in stroke. Stroke 51, 489–497. [PubMed: 31884904]

Bastos-Leite AJ, Kuijer JP, Rombouts SA, Sanz-Arigita E, van Straaten EC, Gouw AA, et al., 2008. Cerebral blood flow by using pulsed arterial spin-labeling in elderly subjects with white matter hyperintensities. AJNR Am. J. Neuroradiol 29, 1296–1301. [PubMed: 18451090]

van Dalen JW, Mutsaerts HJMM, Nederveen AJ, Vrenken H, Steenwijk MD, Caan MWA, et al., 2016. White matter hyperintensity volume and cerebral perfusion in older individuals with hypertension using arterial spin-labeling. AJNR Am. J. Neuroradiol 37, 1824–1830. [PubMed: 27282862]

Bahrani AA, Powell DK, Yu G, Johnson ES, Jicha GA, Smith CD, 2017. White matter hyperintensity associations with cerebral blood flow in elderly subjects stratified by cerebrovascular risk. J. Stroke Cerebrovasc. Dis 26, 779–786. [PubMed: 28063772]

Thomas B, Sheelakumari R, Kannath S, Sarma S, Menon RN, 2019. Regional cerebral blood flow in the posterior cingulate and precuneus and the entorhinal cortical atrophy score differentiate mild cognitive impairment and dementia due to Alzheimer disease. AJNR Am. J. Neuroradiol 40, 1658–1664. [PubMed: 31515217]

Dolui S, Li Z, Nasrallah IM, Detre JA, Wolk DA, 2020. Arterial spin labeling versus 18F-FDG PET to identify mild cognitive impairment. Neuroimage Clin. 25, 102146. [PubMed: 31931403]

Cooper CM, Chin Fatt CR, Liu P, Grannemann BD, Carmody T, Almeida JRC, et al., 2019. Discovery and replication of cerebral blood flow differences in major depressive disorder. Mol. Psychiatry 25, 1500–1510. [PubMed: 31388104]

Alsop DC, Detre JA, Golay X, Günther M, Hendrikse J, Hernandez-Garcia L, et al., 2015. Recommended implementation of arterial spin-labeled perfusion MRI for clinical applications: a consensus of the ISMRM perfusion study group and the European consortium for ASL in dementia. Magn. Reson. Med 73, 102–116. [PubMed: 24715426]

Mutsaerts HJ, Petr J, Václav L, van Dalen JW, Robertson AD, Caan MW, et al., 2017. The spatial coefficient of variation in arterial spin labeling cerebral blood flow images. J. Cereb. Blood Flow Metab 37, 3184–3192. [PubMed: 28058975]

Hendrikse J, van Osch MJ, Rutgers DR, Bakker CJ, Kappelle LJ, Golay X, et al., 2004. Internal carotid artery occlusion assessed at pulsed arterial spin-labeling perfusion MR imaging at multiple delay times. Radiology 233, 899–904. [PubMed: 15486211]

Hirschler L, Munting LP, Khmelinskii A, Teeuwisse WM, Suidgeest E, Warnking JM, et al., 2018. Transit time mapping in the mouse brain using time-encoded PCASL. NMR Biomed. 31.

Liu Y, Zhu X, Feinberg D, Guenther M, Gregori J, Weiner MW, et al., 2012. Arterial spin labeling MRI study of age and gender effects on brain perfusion hemodynamics. Magn. Reson. Med 68, 912–922. [PubMed: 22139957]

Mak HK, Chan Q, Zhang Z, Petersen ET, Qiu D, Zhang L, et al., 2012. Quantitative assessment of cerebral hemodynamic parameters by quasar arterial spin labeling in Alzheimer's disease and cognitively normal elderly adults at 3-tesla. J. Alzheimers Dis 31, 33–44. [PubMed: 22504315]

Eichner C, Jafari-Khouzani K, Cauley S, Bhat H, Polaskova P, Andronesi OC, et al., 2014. Slice accelerated gradient-echo spin-echo dynamic susceptibility contrast imaging with blipped CAIPI for increased slice coverage. Magn. Reson. Med 72, 770–778. [PubMed: 24285593]

Harms MP, Somerville LH, Ances BM, Andersson J, Barch DM, Bastiani M, et al., 2018. Extending the human connectome project across ages: imaging protocols for the lifespan development and aging projects. Neuroimage 183, 972–984. [PubMed: 30261308]

Filley CM, Fields RD, 2016. White matter and cognition: making the connection. J. Neurophysiol 116, 2093–2104. [PubMed: 27512019]

Bookheimer SY, Salat DH, Terpstra M, Ances BM, Barch DM, Buckner RL, et al., 2019. The lifespan human connectome project in aging: an overview. Neuroimage 185, 335–348. [PubMed: 30332613]

Somerville LH, Bookheimer SY, Buckner RL, Burgess GC, Curtiss SW, Dapretto M, et al., 2018. The lifespan human connectome project in development: a large-scale study of brain connectivity development in 5–21 year olds. Neuroimage 183, 456–468. [PubMed: 30142446]

Li X, Wang D, Moeller S, Wang D, Chappell M, Yacoub E, et al., 2018. Pushing the limits of asl imaging for the lifespan human connectome projects. International Society for Magnetic Resonance Imaging.

Andersson JL, Skare S, Ashburner J, 2003. How to correct susceptibility distortions in spin-echo echo-planar images: application to diffusion tensor imaging. Neuroimage 20, 870–888. [PubMed: 14568458]

Smith SM, Jenkinson M, Woolrich MW, Beckmann CF, Behrens TE, Johansen-Berg H, et al., 2004. Advances in functional and structural MR image analysis and implementation as fsl. Neuroimage 23 (Suppl 1), S208–S219. [PubMed: 15501092]

Dale AM, Fischl B, Sereno MI, 1999. Cortical surface-based analysis. I. Segmentation and surface reconstruction. Neuroimage 9, 179–194. [PubMed: 9931268]

Fischl B, Sereno MI, Dale AM, 1999. Cortical surface-based analysis. II: inflation, flattening, and a surface-based coordinate system. Neuroimage 9, 195–207. [PubMed: 9931269]

Greve DN, Fischl B, 2009. Accurate and robust brain image alignment using boundary-based registration. Neuroimage 48, 63–72. [PubMed: 19573611]

Juttukonda MR, Jordan LC, Gindville MC, Davis LT, Watchmaker JM, Pruthi S, et al., 2017. Cerebral hemodynamics and pseudo-continuous arterial spin labeling considerations in adults with sickle cell anemia. NMR Biomed. 30.

Fan AP, Guo J, Khalighi MM, Gulaka PK, Shen B, Park JH, et al., 2017. Long-delay arterial spin labeling provides more accurate cerebral blood flow measurements in moyamoya patients: a simultaneous positron emission tomography/MRI study. Stroke 48, 2441–2449. [PubMed: 28765286]

Lu H, Clingman C, Golay X, van Zijl PC, 2004. Determining the longitudinal relaxation time (t1) of blood at 3.0 tesla. Magn. Reson. Med 52, 679–682. [PubMed: 15334591]

Mahlknecht U, Kaiser S, 2010. Age-related changes in peripheral blood counts in humans. Exp Ther Med 1, 1019–1025. [PubMed: 22993635]

Dai W, Fong T, Jones RN, Marcantonio E, Schmitt E, Inouye SK, et al., 2017. Effects of arterial transit delay on cerebral blood flow quantification using arterial spin labeling in an elderly cohort. J. Magn. Reson. Imaging 45, 472–481. [PubMed: 27384230]

Buijs PC, Krabbe-Hartkamp MJ, Bakker CJ, de Lange EE, Ramos LM, Breteler MM, et al., 1998. Effect of age on cerebral blood flow: measurement with ungated two-dimensional phase-contrast MR angiography in 250 adults. Radiology 209, 667–674. [PubMed: 9844657]

Asllani I, Habeck C, Borogovac A, Brown TR, Brickman AM, Stern Y, 2009. Separating function from structure in perfusion imaging of the aging brain. Hum. Brain Mapp 30, 2927–2935. [PubMed: 19172645]

Ambarki K, Wåhlin A, Zarrinkoob L, Wirestam R, Petr J, Malm J, et al., 2015. Accuracy of parenchymal cerebral blood flow measurements using pseudocontinuous arterial spin-labeling in healthy volunteers. AJNR Am. J. Neuroradiol 36, 1816–1821. [PubMed: 26251434]

Wagner M, Jurcoane A, Volz S, Magerkurth J, Zanella FE, Neumann-Haefelin T, et al., 2012. Age-related changes of cerebral autoregulation: new insights with quantitative t2′-mapping and pulsed arterial spin-labeling MR imaging. AJNR Am. J. Neuroradiol 33, 2081–2087. [PubMed: 22700750]

Taneja K, Liu P, Xu C, Turner M, Zhao Y, Abdelkarim D, et al., 2020. Quantitative cerebrovascular reactivity in normal aging: comparison between phase-contrast and arterial spin labeling MRI. Front Neurol. 11, 758. [PubMed: 32849217]

De Vis JB, Peng SL, Chen X, Li Y, Liu P, Sur S, et al., 2018. Arterial-spin-labeling (ASL) perfusion MRI predicts cognitive function in elderly individuals: a 4-year longitudinal study. J. Magn. Reson. Imaging 48, 449–458. [PubMed: 29292540]

Zhang N, Gordon ML, Goldberg TE, 2017. Cerebral blood flow measured by arterial spin labeling MRI at resting state in normal aging and Alzheimer's disease. Neurosci. Biobehav. Rev 72, 168–175. [PubMed: 27908711]

Parkes LM, Rashid W, Chard DT, Tofts PS, 2004. Normal cerebral perfusion measurements using arterial spin labeling: reproducibility, stability, and age and gender effects. Magn. Reson. Med 51, 736–743. [PubMed: 15065246]

Biagi L, Abbruzzese A, Bianchi MC, Alsop DC, Del Guerra A, Tosetti M, 2007. Age dependence of cerebral perfusion assessed by magnetic resonance continuous arterial spin labeling. J. Magn. Reson. Imaging 25, 696–702. [PubMed: 17279531]

Thomas BP, Liu P, Park DC, van Osch MJ, Lu H, 2014. Cerebrovascular reactivity in the brain white matter: magnitude, temporal characteristics, and age effects. J. Cereb. Blood Flow Metab 34, 242–247. [PubMed: 24192640]

Campbell AM, Beaulieu C, 2006. Pulsed arterial spin labeling parameter optimization for an elderly population. J. Magn. Reson. Imaging 23, 398–403. [PubMed: 16463300]

Smith LA, Melbourne A, Owen D, Cardoso MJ, Sudre CH, Tillin T, et al., 2019. Cortical cerebral blood flow in ageing: effects of haematocrit, sex, ethnicity and diabetes. Eur. Radiol 29, 5549–5558. [PubMed: 30887200]

Liu W, Lou X, Ma L, 2016. Use of 3d pseudo-continuous arterial spin labeling to characterize sex and age differences in cerebral blood flow. Neuroradiology 58, 943–948. [PubMed: 27380039]

Devine B, 1967. Mean Blood Hematocrit of Adults: United states 1960–1962, 11. U.S. Public Health Service.

Zhang N, Gordon ML, Ma Y, Chi B, Gomar JJ, Peng S, et al., 2018. The age-related perfusion pattern measured with arterial spin labeling MRI in healthy subjects. Front Aging Neurosci 10, 214. [PubMed: 30065646]

Lee C, Lopez OL, Becker JT, Raji C, Dai W, Kuller LH, et al., 2009. Imaging cerebral blood flow in the cognitively normal aging brain with arterial spin labeling: implications for imaging of neurodegenerative disease. J. Neuroimaging 19, 344–352. [PubMed: 19292827]

Preibisch C, Sorg C, Förschler A, Grimmer T, Sax I, Wohlschläger AM, et al., 2011. Age-related cerebral perfusion changes in the parietal and temporal lobes measured by pulsed arterial spin labeling. J. Magn. Reson. Imaging 34, 1295–1302. [PubMed: 21953683]

Pavilla A, Arrigo A, Colombani S, Mejdoubi M, 2016. Absolute and regional cerebral perfusion assessment feasibility in head-down position with arterial spin-labeling magnetic resonance. A preliminary report on healthy subjects. J. Neuroradiol 43, 392–397. [PubMed: 27126633]

De Reuck J, 1971. The human periventricular arterial blood supply and the anatomy of cerebral infarctions. Eur. Neurol 5, 321–334. [PubMed: 5141149]

Herman LH, Fernando OU, Gurdjian ES, 1966. The anterior choroidal artery: an anatomical study of its area of distribution. Anat. Rec 154, 95–101. [PubMed: 5922500]

Setsompop K, Cohen-Adad J, Gagoski BA, Raij T, Yendiki A, Keil B, et al., 2012. Improving diffusion MRI using simultaneous multi-slice echo planar imaging. Neuroimage 63, 569–580. [PubMed: 22732564]

Fischl B, Dale AM, 2000. Measuring the thickness of the human cerebral cortex from magnetic resonance images. Proc. Natl. Acad. Sci. U. S. A 97, 11050–11055. [PubMed: 10984517]
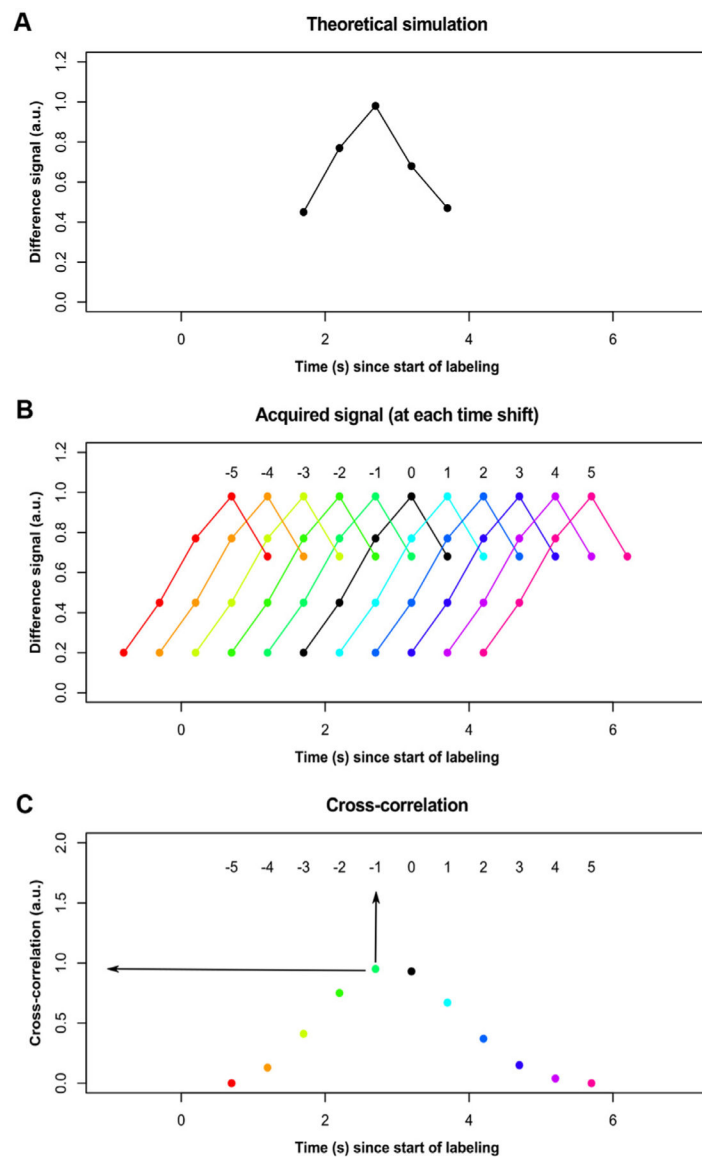
A Theoretical simulation

B Acquired signal (at each time shift)

C Cross-correlation

Fig. 1. Cross-correlation approach.
(**A**) The theoretical kinetic curve based on simulation assuming ATT = 1.2 s is shown after down-sampling to the temporal resolution of the post-labeling delay (PLD) times used. (**B**) The signal for any given voxel (black) is shifted in time – 5 to + 5 in increments of the PLD, and the cross-correlation between the acquired signal and the simulated signal is calculated at each shift. (**C**) Each voxel is then assigned the maximum correlation as well as the time shift at which that correlation is at maximum (arrows).
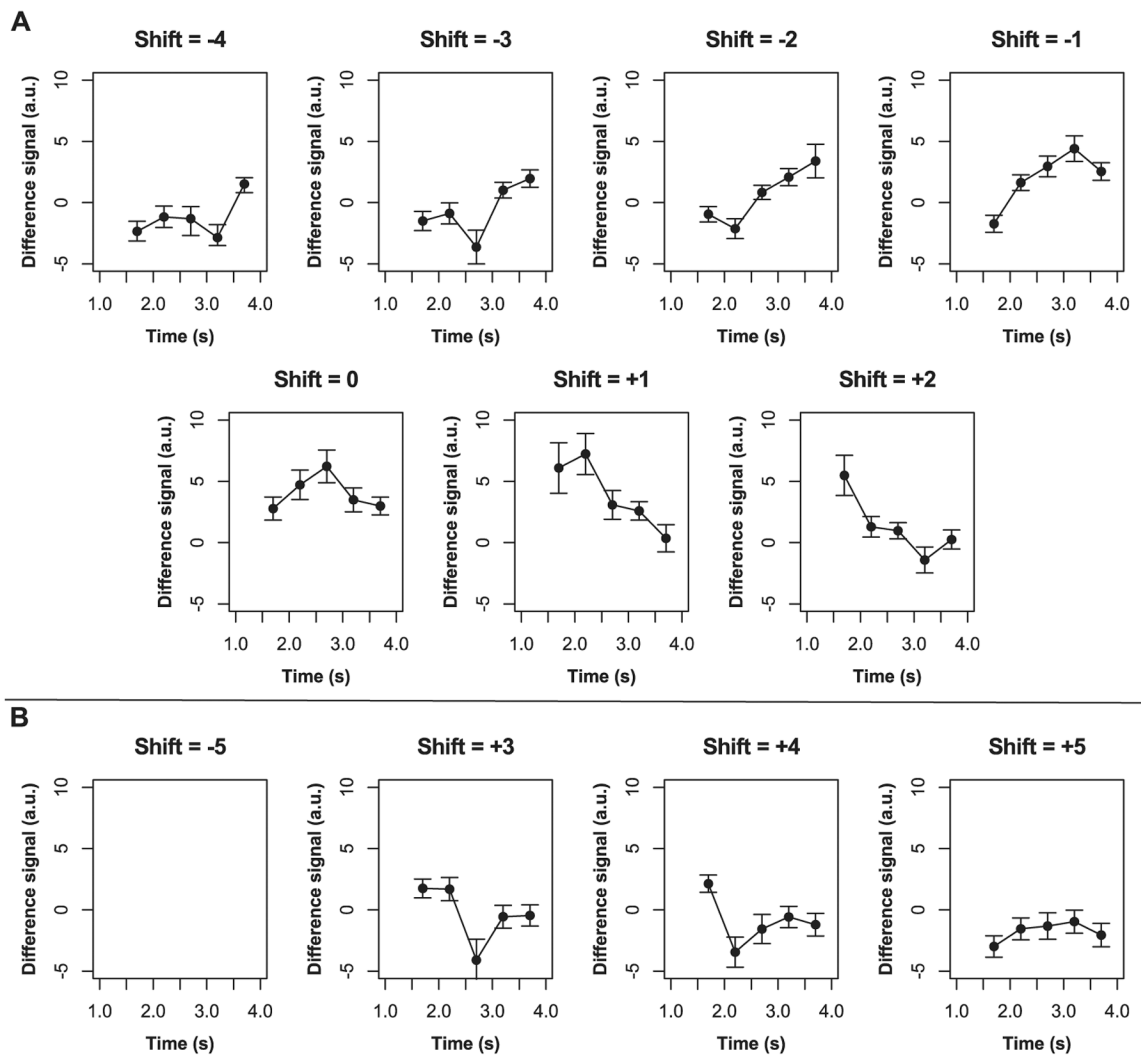
Fig. 2. Signal time courses at various shift indices.

Mean control-label difference signal time courses are shown here across participants for time shifts − 5 to + 5. Error bars represent one standard deviation from the mean.
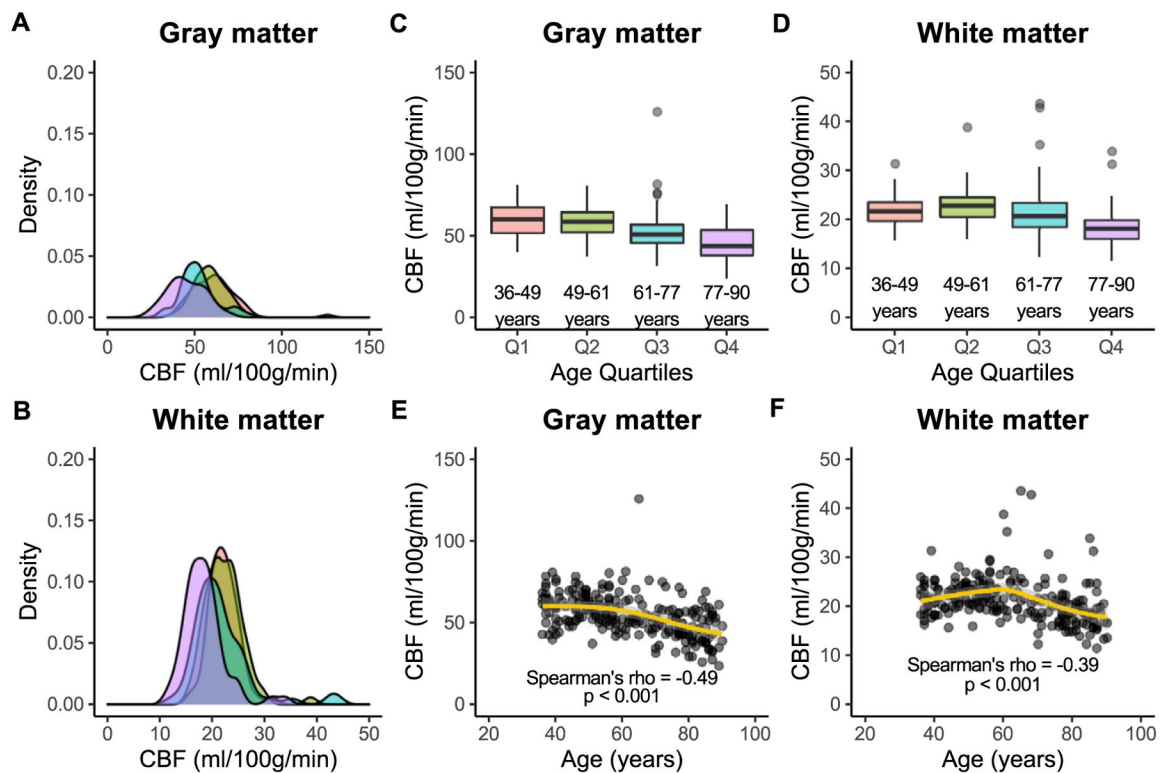
Fig. 3. Cerebral blood flow.
Associations between cerebral blood flow (CBF) and age are shown here in gray and white matter across quartiles of age: Q1 (36–49 years; red), Q2 (49–61 years; green), Q3 (61–77 years; blue), and Q4 (77–90 years; purple). Kernel density plots show that the distribution of gray matter CBF (**A**) is wider than that of white matter (**B**) in all age groups. In addition, gray matter CBF (**C**) is significantly higher than white matter CBF (**D**) in all age groups. Finally, CBF is inversely associated with age in both gray matter (**E**) and white matter (**F**), but this relationship is stronger in gray versus white matter.
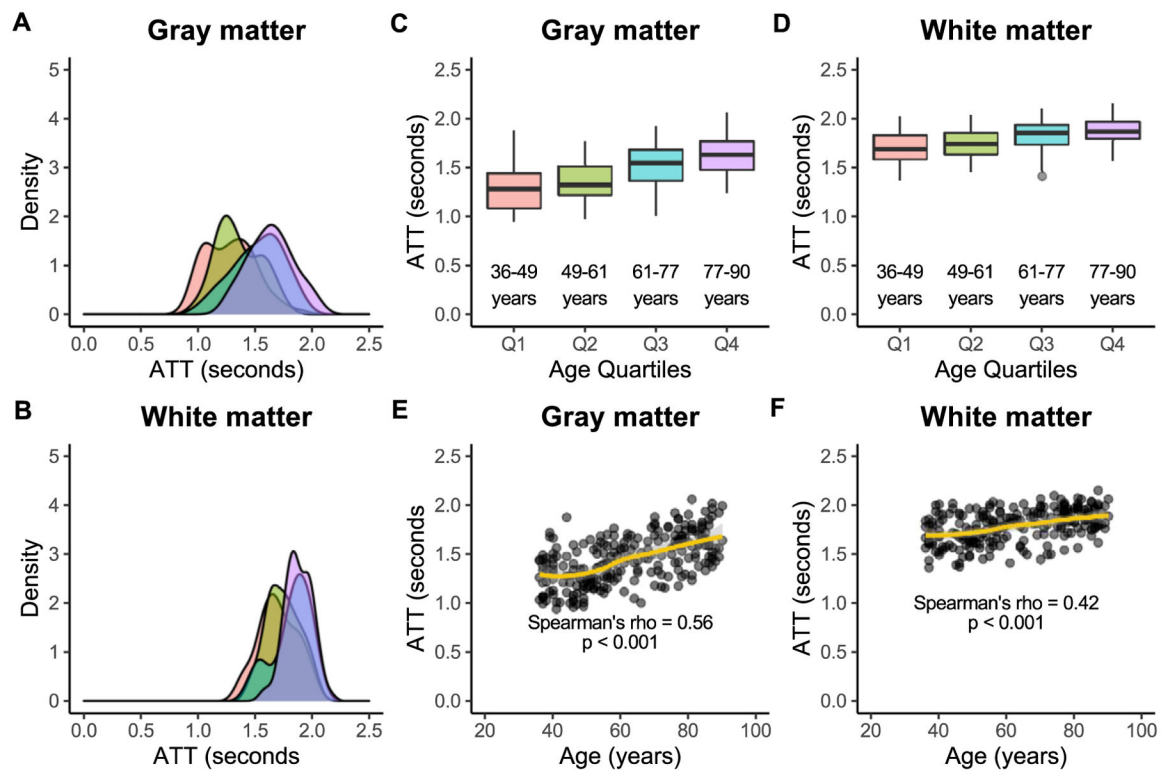
Fig. 4. Arterial transit time.

Associations between arterial transit time (ATT) and age are shown here in gray and white matter across quartiles of age: Q1 (36–49 years; red), Q2 (49–61 years; green), Q3 (61–77 years; blue), and Q4 (77–90 years; purple). Kernel density plots show that the width of the distribution of gray matter ATTs (**A**) may be similar to that of white matter (**B**) across age groups. However, gray matter ATT (**C**) is significantly lower than white matter ATT (**D**) in all age groups. Lastly, ATT is directly associated with age in both gray matter (**E**) and white matter (**F**).
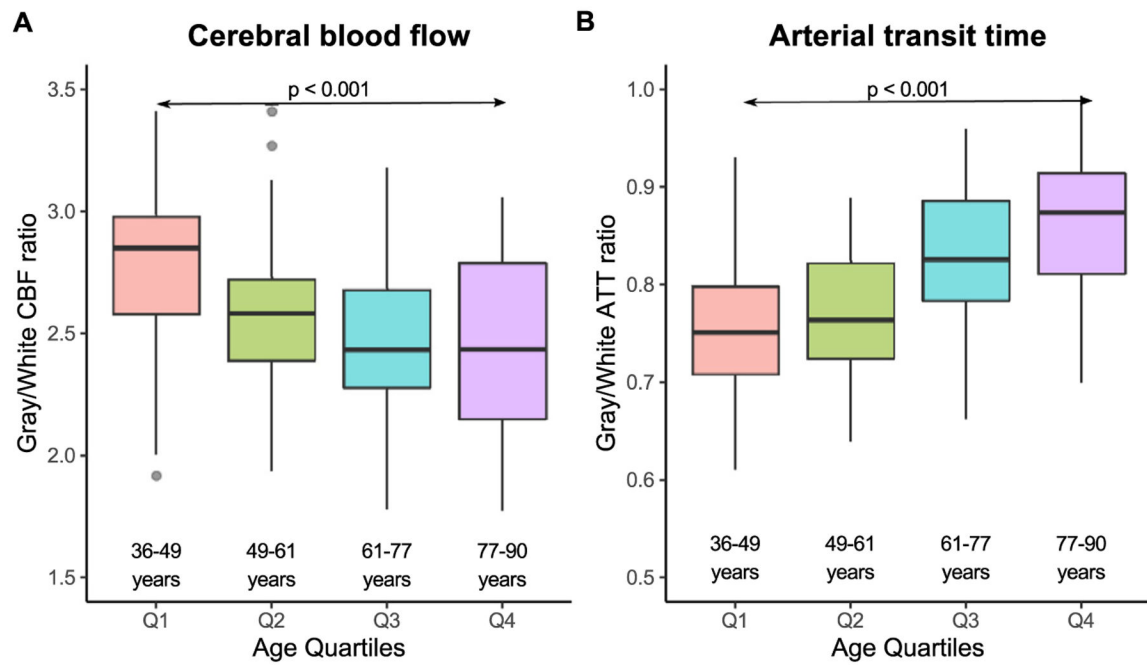
Fig. 5. Gray versus white matter.

Plots of gray-to-white matter CBF (**A**) and gray-to-white ATT (**B**) are shown here for each age quartile. The ratio of gray-to-white matter CBF generally decreases with age ($p < 0.001$) until the 4th quartile in which there is more variability. The ratio of gray-to-white matter ATT generally increases with age ($p < 0.001$).
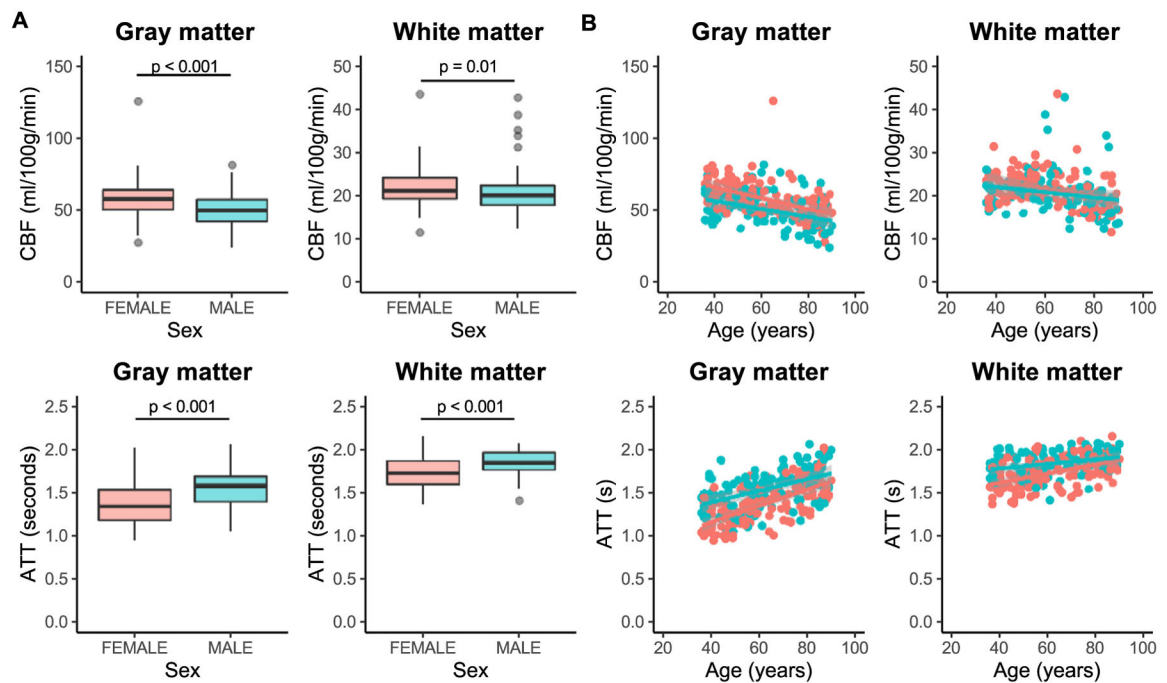
Fig. 6. Sex differences.

Differences in cerebral blood flow (CBF) and arterial arrival time (ATT) between males (blue) and females (red) are shown here. Gray matter CBF ($p < 0.001$) is higher in females compared with males. White matter CBF ($p = 0.01$) was slightly lower in males, but this was not significant after accounting for age (**A; top**). ATT in both gray and white matter is longer ($p < 0.001$) in males than in females (**A; bottom**). Relationships between age and hemodynamics are similar in males and females, with sex differences in CBF and ATT reducing with increasing age (**B**).
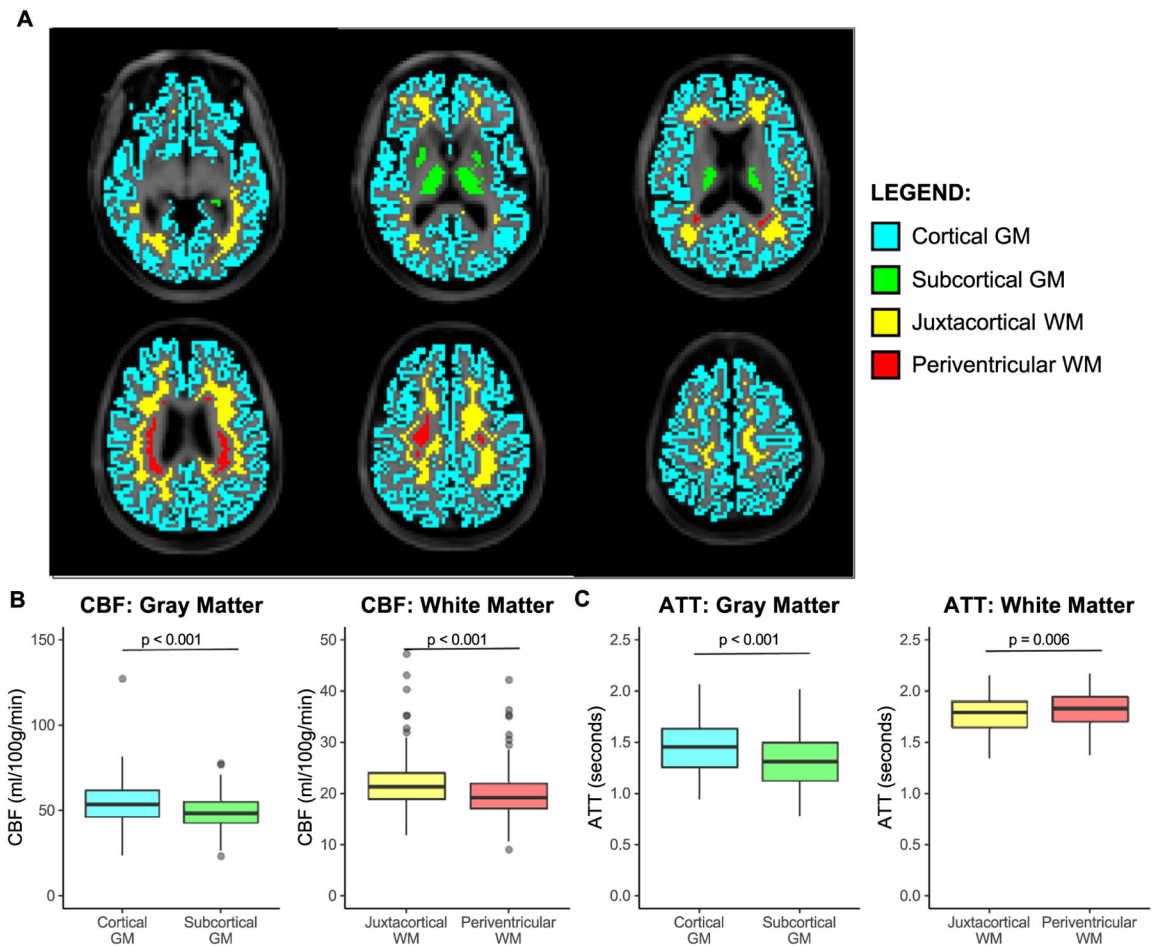
Fig. 7. Tissue subtypes.
Hemodynamic parameters are compared here between various spatial distributions of gray matter (GM) and white matter (WM) shown on T_1-weighted images for six equally spaced axial slices (**A**). Cortical GM (blue), subcortical GM (green), juxtacortical WM (yellow), and periventricular WM (red) regions were used. CBF is higher in cortical versus subcortical GM and in juxtacortical versus periventricular WM (**B**). ATT is longer in cortical versus subcortical GM and in periventricular versus juxtacortical WM (**C**).
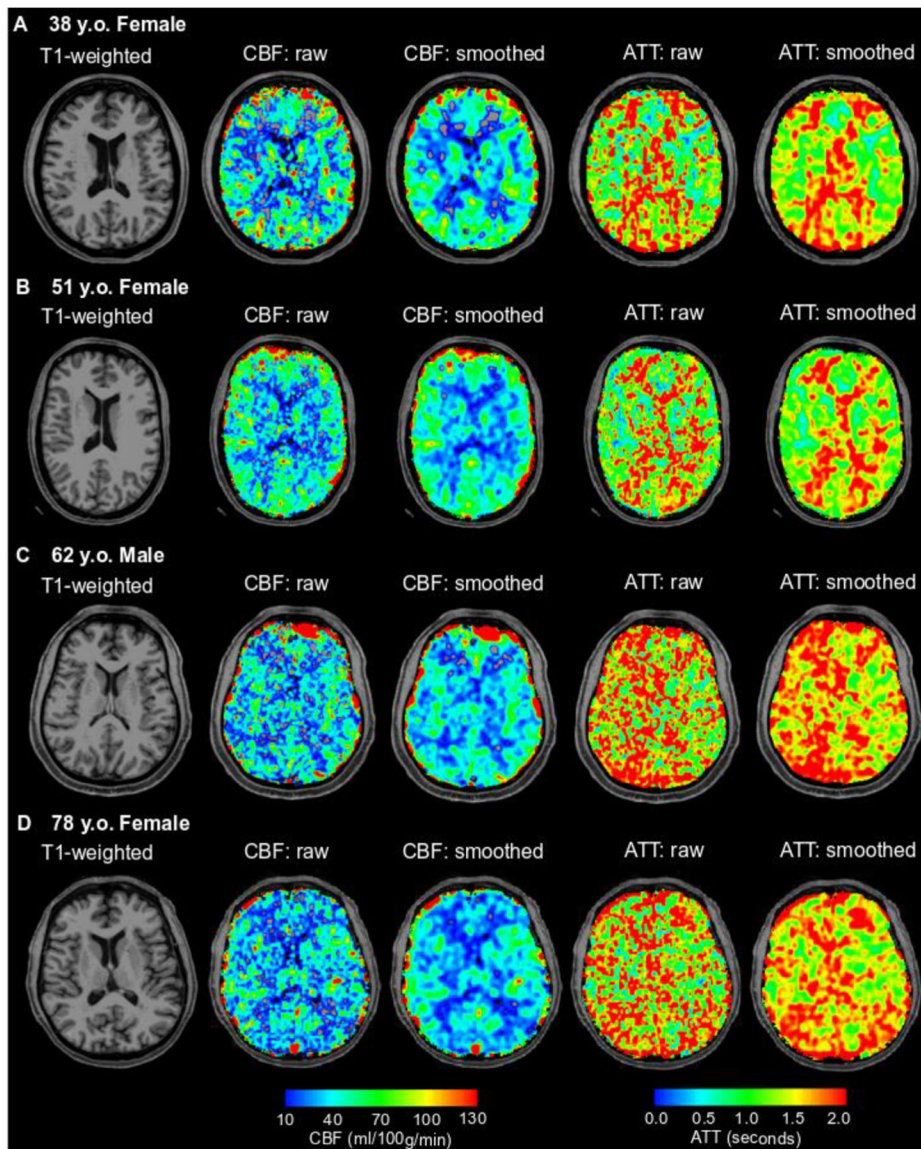
Fig. 8. Representative examples.

T_1-weighted (column 1) cerebral blood flow (CBF; columns 2 and 3), and arterial transit time (ATT; columns 4 and 5) are shown here for study participants across each quartile of age: 38 y.o. female (Q1; A), 51 y.o. female (Q2; B), 62 y.o. male (Q3; C), and 78 y.o. female (Q4; D). In addition to CBF and ATT images without any smoothing (raw), which are the basis for the quantifications reported in this manuscript, images smoothed with a 3.75 mm kernel are also shown for visualization of the gray-to-white matter contrast expected from conventional ASL CBF images. The overall group-level findings of this study of decreasing CBF and increasing ATT with age in the gray and white matter can be visualized on a subject-level as observed in these representative cases.

Table 1

Summary of demographic variables.

	Participants ($n = 234$)
Age	Median: 61 years
	Interquartile range: 49–77 years
	Full range: 36–90 years
Sex	Female: 55.6%
	Male: 44.4%
Race	Caucasian: 71.4%
	African American: 16.2%
	Asian: 7.3%
	More than one: 3.8%
	Unknown or not reported: 1.3%
Ethnicity	Hispanic or Latino: 11.1%
	Not Hispanic or Latino: 88.5%
	Unknown or not reported: 0.4%
Medication Use	Prevalence: 62.3%
	Average number of medications: 3.2
	Anti-hypertensives: 25.2%